

# Localisation for a line defect in an infinite square lattice

D.J. Colquitt<sup>1</sup>, M.J. Nieves<sup>2</sup>, I.S. Jones<sup>2</sup>, A.B. Movchan<sup>1</sup>, and N.V. Movchan<sup>1</sup>

<sup>1</sup>*Department of Mathematical Sciences, University of Liverpool, Liverpool L69 3BX, U.K.*

<sup>2</sup>*School of Engineering, John Moores University, James Parsons Building, Byrom Street, Liverpool L3 3AF, U.K.*

## Abstract

Localised defect modes generated by a finite line defect composed of several masses, contained inside an infinite square cell lattice, are analysed using the linear superposition of Green's function for a single mass defect. For a nontrivial solution, it is shown that this problem can be reduced to a characteristic equation involving the eigenfrequencies for the defect and the mass of the particles composing the defect. An example is presented where eigenfrequencies linked to this system and the corresponding eigenmodes are computed for a defect composed of several particles. An infinite chain of defects contained in the infinite square lattice is also considered and an explicit dispersion relation is obtained. For the case when the number of masses within the line defect is large, it is shown that the range of the eigenfrequencies can be predicted using the dispersion diagram for the infinite chain.

## 1 Introduction

Localisation of waves due to an infinite chain strata acting as a defect within an infinite square lattice, has been considered in the [1]. For the case of an infinite chain of masses embedded into a square lattice, dispersion relations can be computed in the explicit form, and hence waveguide modes localised around the chain of masses can be analysed.

A theory and a detailed discussion of applications for dynamic lattice problems involving cracks modelled as semi-infinite faults, for both square and triangular elastic lattices, are presented in [2]. In [3], for a structured interface and a crack propagating with constant speed within a square lattice, localised modes were analysed. In particular, the crack propagation can be supported by a sinusoidal wave localised along the crack, known as a *knife wave*. Using the lattice model, the dispersion relations for the crack within the square lattice can be derived. As shown in numerical experiments, these relations allow for the prediction of the average crack speed within the lattice when a fracture criterion for the crack path bonds is introduced.

For the finite-frequency regime, a theory of asymptotic homogenisation for square-cell lattices has been developed in [4]. This theory makes use of information related to standing wave modes found in the lattice problem. Then a two-scale asymptotic procedure can be applied in order to obtain an effective partial differential equation for the corresponding macroscale that contains information about its microscale.

Point forces acting at stop-band frequencies within square and triangular lattices have been shown to produce localised primitive wave forms within the lattice [5]. Similar localised primitive waveforms were demonstrated for the in plane motion of elastic lattices in [6]. The shape of these waveforms, created by a point force, were linked to the dispersive properties of Bloch waves in the lattice.

Green's kernels describing wave propagation within an infinite square lattice, caused by a point source, have been studied in [7]. The resulting solution was analysed for frequencies within the pass band and the corresponding asymptotics at infinity were also obtained.

When the frequency is located in the stop band, for several classes of continuous and discrete models localised defect modes have been identified when a mass variation within the structure is made. For a particular choice of the mass variation, these defect modes can then be linked to stop-band Green's kernel which can be used in the construction of the defect modes as in [8].

Classical applications in the theory of defects in crystals and dislocations follow from the fundamental work [9], where explicit closed form solutions were derived for a heterogeneous lattice system when two distant particles of different masses interchange their position. More recently, the envelope function based perturbation approach was developed in [10] and [11] for analysis of waveguides in photonic crystal structures. In the latter case, an array of cylinders (inclusions) represents a waveguide within a two-dimensional structure, and the frequencies of the guided modes are close to the band edge of the unperturbed doubly periodic system.

The structure of this paper is as follows. In section 2, the problem of a finite line of defects (created by a perturbation of point masses), embedded in an infinite square lattice is considered. Several representations for Green's matrix are presented, including integral forms and representation in terms of a generalised hypergeometric function. Localised defect modes for the finite line are analysed in section 2.1. Therein, the necessary and sufficient condition for the existence of localised modes is formulated, and asymptotic expansions, in the far field and at the band edge, are also presented. Illustrative examples for a finite number of defects are given in section 2.2, where eigenfrequencies and eigenmodes are presented and compared with asymptotic results from the previous section. The analysis of a finite sized defect region is accompanied by the waveguide modes that may exist in a lattice containing an infinite chain of point masses, as in section 3. The governing equations for such a waveguide and solvability of the problem are discussed in sections 3.1 and 3.2, 3.3. In section 3.4, the dispersion relation corresponding to the localised mode for the infinite chain is given. Finally, in section 4, a numerical simulation illustrates that the solution of the problem of the infinite chain can be used to predict the range of eigenfrequencies of localised modes for a finite but sufficiently long array of masses representing a rectilinear defect in a square lattice.

## 2 A finite inclusion in an infinite square lattice

Consider a square meshing of  $\mathbb{R}^2$  such that the position of node  $\mathbf{n} \in \mathbb{Z}^2$  is simply given by  $\mathbf{n}$ . Let there be  $N$  defects (with  $N \in \mathbb{N}_0$ ) distributed along  $n_2 = 0$  as shown in figure 1. The defects are characterised by a reduction in mass by a factor of  $1 - r$  (and hence a mass of  $0 \leq r \leq 1$ ).

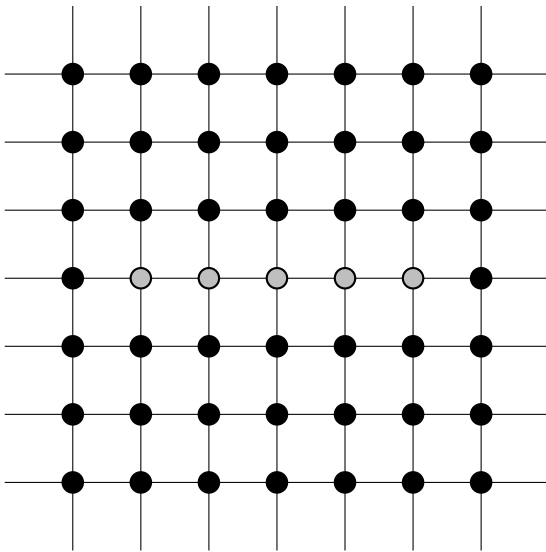


**Figure 1:** A finite line of defects in an infinite square lattice. The length of the links, the stiffness of the bonds and the mass of the [black] nodes are taken as natural units.

Let  $u_{\mathbf{n}}$  denote the complex amplitude of the time-harmonic out of plane displacement of node

$\mathbf{n}$ . Then, the equations of motion are

$$u_{\mathbf{n}+\mathbf{e}_1} + u_{\mathbf{n}-\mathbf{e}_1} + u_{\mathbf{n}+\mathbf{e}_2} + u_{\mathbf{n}-\mathbf{e}_2} + (\omega^2 - 4)u_{\mathbf{n}} = (1-r)\omega^2 \delta_{0,n_2} \sum_{p=0}^{N-1} u_{\mathbf{n}} \delta_{p,n_1}, \quad (1)$$

where  $\omega$  is the radian frequency and  $\mathbf{e}_i = [\delta_{1,i}, \delta_{2,i}]^T$  and  $\delta_{i,j}$  is the Kronecker Delta. By means of the discrete Fourier Transform

$$\mathcal{F}: u_{\mathbf{n}} \mapsto u^{\text{FF}}(\boldsymbol{\xi}) = \sum_{\mathbf{n} \in \mathbb{Z}^2} u_{\mathbf{n}} e^{-i\mathbf{n} \cdot \boldsymbol{\xi}}, \quad (2)$$

the governing equation (1) may be written

$$(\omega^2 - 4 + 2 \cos \xi_1 + 2 \cos \xi_2) u^{\text{FF}}(\boldsymbol{\xi}) = \sum_{p=0}^{N-1} u_{p,0} e^{-ip\xi_1}. \quad (3)$$

Inverting the transform yields the discrete field

$$u_{\mathbf{n}}(\omega) = (1-r)\omega^2 \sum_{p=0}^{N-1} u_{p,0} g(\mathbf{n}, p; \omega), \quad (4)$$

where  $g(\mathbf{n}, p; \omega)$  is the shifted Green's matrix defined as:

$$g(\mathbf{n}, p; \omega) = \frac{1}{\pi^2} \int_0^\pi \int_0^\pi \frac{\cos([n_1 - p]\xi_1) \cos(n_2 \xi_2)}{\omega^2 - 4 + 2 \cos \xi_1 + 2 \cos \xi_2} d\xi_1 d\xi_2. \quad (5)$$

For the purposes of numerical evaluation and asymptotic analysis in the stop band of the ambient lattice ( $\omega^2 > 8$ ), it is convenient to rewrite the Green's matrix as a single integral

$$g(\mathbf{n}, p; \omega) = \frac{1}{2\pi} \int_0^\pi \frac{(\sqrt{a^2 - 1} - a)^{|n_1 - p|}}{\sqrt{a^2 - 1}} \cos(n_2 \xi_2) d\xi_2, \quad (6)$$

where  $a = \omega^2/2 - 2 + \cos \xi_2$ . Reversing the order of integration yields the same result, but with  $n_1 - p$  and  $n_2$  interchanged, and  $\xi_1$  interchanged with  $\xi_2$ . An alternative representation can be found in [12] among others

$$g(\mathbf{n}, p; \omega) = \frac{(-1)^{n_1 - p + n_2}}{2} \int_0^\infty I_{n_1 - p}(x) I_{n_2}(x) e^{-\alpha x} dx, \quad (7)$$

where  $I_m(x)$  is the modified Bessel function of the first kind,  $\alpha = \omega^2/2 - 2 > 2$ . The integral is symmetric about  $n_1 - p = 0$  and  $n_2 = 0$  and therefore it may be assumed, without loss of generality, that  $n_1 \geq p$  and  $n_2 \geq 0$ . The integral (7) may then be represented in terms of a regularised generalised hypergeometric function (see [13] equation 8, section 3.15.6)

$$g(\mathbf{n}, p; \omega) = \frac{(-1)^{m+n_2}}{(2\alpha)^{1+m+n_2}} ((m+n_2)!)^2 \times {}_4F_3 \left[ \begin{matrix} (1+m+n_2)/2, (1+m+n_2)/2, (2+m+n_2)/2, (2+m+n_2)/2 \\ 1+m, 1+n_2, 1+m+n_2 \end{matrix}; \frac{4}{\alpha^2} \right], \quad (8)$$

where  $m = n_1 - p$ . The series (8) is convergent for  $\alpha^2 > 4$ , that is, everywhere in the stop band of the ambient lattice.

## 2.1 Localised modes

Of primary interest are localised modes, that is, modes of vibration at frequencies that are not supported in the ambient lattice and therefore decay rapidly away from the defect sites. Introducing the vector  $\mathcal{U} = [u_{0,0}, u_{2,0}, \dots, u_{N-1,0}]^T$  and choosing  $n_2 = 0$  in equation (4) yields the eigenvalue problem

$$\mathcal{U} = (1 - r)\omega^2 \mathcal{G}(\omega) \mathcal{U}, \quad (9)$$

where the matrix entries  $[\mathcal{G}(\omega)]_{ij} = g(i - 1, 0, j - 1; \omega)$ . Clearly,  $\mathcal{G}$  is symmetric and Toeplitz (and hence bisymmetric and centrosymmetric)

$$\mathcal{G} = \begin{pmatrix} \mathcal{G}_{11} & \mathcal{G}_{12} & \mathcal{G}_{13} & \cdots & \mathcal{G}_{1(N-1)} & \mathcal{G}_{1N} \\ & \mathcal{G}_{11} & \mathcal{G}_{12} & \cdots & \mathcal{G}_{1(N-2)} & \mathcal{G}_{1(N-1)} \\ & & \mathcal{G}_{11} & \cdots & \mathcal{G}_{1(N-3)} & \mathcal{G}_{1(N-2)} \\ & & & \ddots & \vdots & \vdots \\ & & & & \mathcal{G}_{11} & \mathcal{G}_{12} \\ & & & & & \mathcal{G}_{11} \end{pmatrix}, \quad (10)$$

which greatly reduces the number of required computations. Indeed, for  $N$  defects the matrix  $\mathcal{G}$  has  $N$  independent elements. The solvability condition of the spectral problem (9) yields a transcendental equation in  $\omega$ ,

$$\det [\mathbb{I}_N - (1 - r)\omega^2 \mathcal{G}] = 0, \quad (11)$$

where  $\mathbb{I}_N$  is the  $N \times N$  identity matrix. Equation (11) is the necessary and sufficient condition for the existence of a localised mode. Symmetry implies that there exists an orthonormal set of  $N$  eigenvectors of  $\mathcal{G}$  and hence,  $N$  eigenvalues (frequencies). The centrosymmetry of  $\mathcal{G}$  allows the number of symmetric and skew-symmetric modes to be determined [14]. Introducing the  $N \times N$  exchange matrix

$$\mathbb{J}_N = \begin{pmatrix} 0 & 0 & 0 & 1 \\ 0 & 0 & 1 & 0 \\ 0 & \ddots & 0 & 0 \\ 1 & 0 & 0 & 0 \end{pmatrix}, \quad (12)$$

an eigenmode is said to be symmetric if  $\mathcal{U} = \mathbb{J}_N \mathcal{U}$  and skew-symmetric if  $\mathcal{U} = -\mathbb{J}_N \mathcal{U}$ . For a system of  $N$  defects there exist  $\lceil N/2 \rceil$  symmetric modes and  $\lfloor N/2 \rfloor$  skew-symmetric modes, where  $\lceil \cdot \rceil$  and  $\lfloor \cdot \rfloor$  are the ceiling and floor operators respectively. Of course here, symmetry refers to the symmetry of the eigenmodes in the  $n_1$  direction about the centre of the defect line. Due to the symmetry of the system, all modes are symmetric about the line  $n_2 = 0$ .

Consider the total force on an inclusion containing  $N$  defects

$$F = \sum_{p=0}^{N-1} (u_{p-1,0} + u_{p+1,0} + 2u_{p,1}). \quad (13)$$

By definition, for a skew-symmetric mode  $u_{p,0} = -u_{N-1-p,0}$  and further  $u_{p,q} = -u_{N-1-p,q}$ . Hence, for all skew-symmetric modes the inclusion is self-balanced (i.e.  $F = 0$ ) and therefore, all skew-symmetric localised modes can be considered as multipole modes.

For the illustrative examples presented later, the eigenvalue problem (9) will be solved for the unit eigenvectors ( $|\mathcal{U}| = 1$ ).

**2.1.1 Asymptotics** Here, asymptotics are considered for some particular cases. Asymptotic expansions for an isolated Green's matrix in various configurations have been considered in [8] and the approach detailed therein is used here.

**In the far field, along the line of defects.** The case of  $n_1 \rightarrow \infty$ ,  $n_2 = 0$  and finite  $N$  is considered. It is observed that at large  $n_1$  and sufficiently small  $N$ , the dominant contribution to the integral (6) comes from a small region in the vicinity of  $\xi = \pi$ . Therefore,

$$\cos \xi_2 \sim -1 + \frac{1}{2}(\pi - \xi_2)^2, \quad a \sim c + \frac{1}{2}(\pi - \xi_2)^2 \quad \text{and} \quad (14)$$

$$\sqrt{a^2 - 1} \sim \sqrt{c^2 - (\pi - \xi_2)^4/4 - (\pi - \xi_2)^2} = \sqrt{c^2 - 1} + c \frac{(\pi - \xi_2)^2}{2\sqrt{c^2 - 1}} \quad (15)$$

where  $c = \omega^2/2 - 3$ . Thus,

$$\left\{ \sqrt{a^2(\xi_2) - 1} - a(\xi_2) \right\}^{|n_1 - p|} \sim \left( \sqrt{c^2 - 1} - c \right)^{|n_1 - p|} \exp \left[ -|n_1 - p| \frac{(\pi - \xi_2)^2}{2\sqrt{c^2 - 1}} \right]. \quad (16)$$

Hence, for  $0 < \epsilon \ll 1$  and making use of (6)

$$g(n_1, 0, p, \omega) \sim \frac{\left( \sqrt{c^2 - 1} - c \right)^{|n_1 - p|}}{2\pi\sqrt{c^2 - 1}} \int_{\pi - \epsilon}^{\pi} \exp \left[ -|n_1 - p| \frac{(\pi - \xi_2)^2}{2\sqrt{c^2 - 1}} \right] d\xi_2. \quad (17)$$

Making the substitution

$$x = (\pi - \xi_2) \sqrt{\frac{|n_1 - p|}{2\sqrt{c^2 - 1}}}, \quad (18)$$

and performing the resulting integration yields

$$g(n_1, 0, p; \omega) \sim \frac{\left( \sqrt{c^2 - 1} - c \right)^{|n_1 - p|}}{\sqrt{8\pi\sqrt{c^2 - 1}}} \frac{1}{\sqrt{|n_1 - p|}} \quad \text{as } n_1 \rightarrow \infty. \quad (19)$$

Thus, the physical field has the following approximate representation for  $n_1 \rightarrow \infty$

$$u_{n_1, 0}(\omega) \sim (1 - r)\omega^2 \sum_{p=0}^{N-1} \frac{\left( \sqrt{c^2 - 1} - c \right)^{|n_1 - p|}}{\sqrt{8\pi\sqrt{c^2 - 1}}} \frac{u_{p, 0}(\omega)}{\sqrt{|n_1 - p|}}, \quad (20)$$

where  $u_{p' - p, 0}(\omega)$  should be determined from (9). It is observed that when  $N = 1$  equation (20) is consistent with equation (4.17) in [8] up to a change in sign.

**In the far field, perpendicular to the line of forces.** Here, the case considered is  $n_1 = p'$ ,  $n_2 \rightarrow \infty$  with  $N$  and  $p'$  finite. The method used here follows the same general procedure as the previous case. However in this case, the kernel is oscillatory and is therefore approximated as a product of decaying and oscillatory functions.

For sufficiently small  $p' - p$  and large  $n_2$ , the non-oscillatory part of the integrand in (6) is approximated as before leading to

$$g(0, n_2; p) \sim \frac{\left( \sqrt{c^2 - 1} - c \right)^{|n_2|}}{2\pi\sqrt{c^2 - 1}} \int_{\pi - \epsilon}^{\pi} \exp \left[ -|n_2| \frac{(\pi - \xi_1)^2}{2\sqrt{c^2 - 1}} \right] \cos([p' - p]\xi_1) d\xi_1. \quad (21)$$

Making a similar change of variable

$$x = (\pi - \xi_1) \sqrt{\frac{|n_2|}{2\sqrt{c^2 - 1}}}, \quad (22)$$

and integrating, it is found that

$$g(p', n_2, p; \omega) \sim (-1)^{(p'-p)} \frac{(\sqrt{c^2-1}-c)^{|n_2|}}{\sqrt{8\pi\sqrt{c^2-1}}} \frac{1}{\sqrt{|n_2|}} \exp \left[ -(p'-p)^2 \frac{\sqrt{c^2-1}}{2|n_2|} \right], \quad (23)$$

Hence, for  $n_2 \rightarrow \infty$  the physical field may be approximated by

$$u_{p', n_2}(\omega) \sim (1-r)\omega^2 \sum_{p=0}^{N-1} (-1)^{(p'-p)} \frac{(\sqrt{c^2-1}-c)^{|n_2|}}{\sqrt{8\pi\sqrt{c^2-1}}} \exp \left[ -(p'-p)^2 \frac{\sqrt{c^2-1}}{2|n_2|} \right] \frac{u_{p,0}(\omega)}{\sqrt{|n_2|}} \quad (24)$$

It is observed that for  $N=1$  and  $p'=p$ , the above equation (24) is consistent with equation (4.17) in [8] up to a change in sign. Moreover, for the case of  $p'=p$  (24) reduces to (20).

**2.1.2 Near the band edge** The representations of Green's matrix (6)-(8) presented in the previous sections are valid in the stop band. However, given that the hypergeometric function in the representation (8) is zero balanced<sup>1</sup> the stop band Green's matrix can be extended into the pass band by analytic continuation. In particular, the analytical continuation of the function (8) has the form [15]

$$\begin{aligned} g(\mathbf{n}, p; \omega) = & \frac{(-4)^{m+n_2}}{\pi(2\alpha)^{1+m+n_2}} \\ & \sum_{j=0}^{\infty} \left( \frac{([1+m+n_2]/2)_j}{j!} \right)^2 \left\{ \sum_{k=0}^j \frac{(-j)_k}{\{([1+m+n_2]/2)_j\}^2} \mathfrak{F}(m, n_2, k) [\psi(1+j-k) \right. \\ & \left. + \psi(1+j) - \psi([1+m+n_2]/2+j) - \log \left( 1 - \frac{4}{\alpha^2} \right) \right] \\ & \left. + (-1)^j (j)! \sum_{k=j+1}^{\infty} \frac{(k-j-1)!}{\{([1+m+n_2]/2)_k\}^2} \mathfrak{F}(m, n_2, k) \right\} \left( 1 - \frac{4}{\alpha^2} \right)^j \end{aligned} \quad (25)$$

where  $(\cdot)_j$  is the Pochhammer symbol,  $\psi(x)$  is the Digamma function, and

$$\mathfrak{F}(m, n, k) = \frac{(m)_k (n)_k}{k!} {}_3F_2 \left[ \begin{matrix} (m+n_2)/2, (m+n_2)/2, -k \\ m, n \end{matrix} ; 1 \right]. \quad (26)$$

Hence, choosing  $j=0$  yields the leading order behaviour of (8) in the neighbourhood of  $\alpha^2 = 4$  ( $\omega \rightarrow \sqrt{8}$ )

$$\begin{aligned} g(\mathbf{n}, p; \omega) \sim & \frac{(-4)^{m+n_2}}{\pi(2\alpha)^{1+m+n_2}} \left\{ \left[ -2\gamma - \psi([1+m+n_2]/2) \right. \right. \\ & \left. \left. - \log \left( 1 - \frac{4}{\alpha^2} \right) \right] + \sum_{k=1}^{\infty} \frac{(k-1)!}{\{([1+m+n_2]/2)_k\}^2} \mathfrak{F}(m, n_2, k) \right\}, \end{aligned} \quad (27)$$

where  $\gamma$  is the Euler-Mascheroni constant. Alternative representations of (27) and leading order continuations for general zero-balanced  ${}_q F_q$  can be found in [16]. Since  $k > 0$ , the series representation of the hypergeometric function in (26) has a finite number of terms and therefore

<sup>1</sup> Indeed, any integer balanced hypergeometric function  ${}_q F_q$  can be analytically continued to the boundary of the unit disk. See [15] for details.

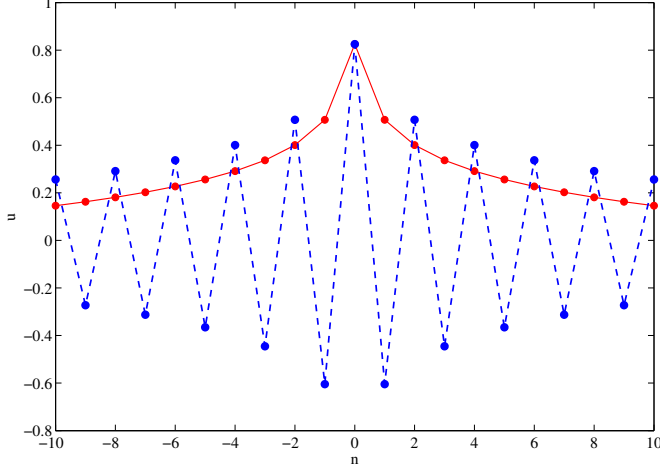


**Figure 2:** The solid red curve shows the asymptotic expression for the displacement field along the diagonal in the vicinity of the band edge (cf. equation (28b)). The dashed blue curve shows the corresponding asymptotic expression for the field along the bond line (cf. equation (28a)). The frequency chosen was  $\omega = 2.829$ .

may be computed exactly. The convergence condition for the infinite sums in (25) (and (27)) is  $2 + m + n_2 + j > 0$ , and is automatically satisfied since it was assumed (without loss of generality) at the outset that  $m > 0$  and  $n_2 > 0$ .

The asymptotic expression (27) is particularly interesting as it elucidates the nature of the singularity of the lattice Green's matrix at the band edge. In particular, the asymptotic representation (27) captures the logarithmic singularity as  $\omega \rightarrow \sqrt{8}$ . This logarithmically singular behaviour near the band edge is not obvious from the original representations presented earlier (cf. equations (6)-(8)).

For the cases of  $n_2 = 0$  (or  $m = 0$ ) and  $m = n_2$ , equation (27) reduces to the following simplified forms. Along bond lines ( $n_2 = 0$ ):

$$g(n_1, 0, p; \omega) \sim \frac{(-4)^{1+m}}{\pi(2\alpha)^{1+m}} \left[ 2\gamma + \psi([1+m]/2) + \log\left(1 - \frac{4}{\alpha^2}\right) \right], \quad (28a)$$

and along the diagonal rays  $m = n_2$ :

$$g(m, m, p; \omega) \sim -\frac{16^m}{\pi(2\alpha)^{1+2m}} \left[ 2\gamma + \psi(1/2 + m) + \log\left(1 - \frac{4}{\alpha^2}\right) \right], \quad (28b)$$

where the reader is reminded that  $m = n_1 - p$ . The Digamma function grows logarithmically as  $m \rightarrow \infty$  and the term  $2\gamma + \psi(1/2 + m)$  is strictly positive for  $m > 0$ . Therefore, for sufficiently small  $m$  the bracketed term in equation (28) is negative in the neighbourhood of  $\alpha = 2$ . Hence, in the vicinity of the band edge, Green's matrix exhibits fundamentally different behaviour along the bond lines compared with the diagonal rays. In particular, along the bond lines the masses will oscillate out of phase, whereas for the diagonal ray lines the masses will oscillate in phase, as illustrated in figure 2. In the far field, equations (28) further reduce to

$$g(n_1, 0, p; \omega) \sim \frac{(-4)^{1+m}}{\pi(2\alpha)^{1+m}} \left[ 2\gamma + \log\left(\frac{m}{2}\right) + \log\left(1 - \frac{4}{\alpha^2}\right) \right] \quad \text{as } n_2 \rightarrow \infty, \quad (29a)$$

$$g(m, m, p; \omega) \sim -\frac{16^m}{\pi(2\alpha)^{1+2m}} \left[ 2\gamma + \log m + \log\left(1 - \frac{4}{\alpha^2}\right) \right] \quad \text{as } m \rightarrow \infty. \quad (29b)$$

## 2.2 Illustrative examples

Several particular cases are considered here corresponding to  $N \in [1, 3]$ . The red curves in figure 3 show the  $(\omega, r)$  values for which the sufficient condition for a localised mode (cf. equation (11)) is satisfied. The grey dashed lines show the line of demarcation between the pass and stop bands of

the ambient lattice. The ambient lattice supports propagating waves at frequencies to the left of this line ( $\omega < \sqrt{8}$ ). The blue curves correspond to the problem of a chain of  $N$  particles of mass  $r$ , connected by springs to two nearest neighbours and rigid foundations above and below. For such a problem, the out of plane displacement of mass  $n \in \mathbb{Z}$  satisfies

$$\mathcal{L} \begin{bmatrix} v_0 \\ v_1 \\ \vdots \\ v_{N-1} \end{bmatrix} = 0, \quad (30)$$

where the matrix  $L$  has elements

$$[\mathcal{L}]_{ij} = (r\omega^2 - 4)\delta_{ij} + \delta_{i-1,j} + \delta_{i,j-1}. \quad (31)$$

The blue curves represent the solutions of the solvability condition:  $\det L = 0$ . It is observed that as  $\omega \rightarrow \infty$ , the blue curves approach the red curves from below. It is interesting to note that, in contrast to the 1D and 3D cases [9], the image of  $r(\omega)$  is  $(0, 1]$ . In other words, a localised defect mode can be initiated by creating a defect in the lattice by removing any amount of mass from one or more nodes. In 1D and 3D lattices, there is some upper bound on the mass of the defect such that a localised mode can be initiated. As  $r \rightarrow 1$ , that is, the lattice approaches a homogeneous lattice, the frequency of the localised mode approaches the band edge ( $\omega \rightarrow \sqrt{8}$ ).

In addition, it is also observed that for  $N > 1$ , the red curves intersect the band edge at several unique values of  $r$ . This suggests that for a given number of defects, there exists a maximum value of  $r$  below which all possible localised eigenmodes may be initiated. Above this value of  $r$  it is only possible to initiate a subset of the possible eigenmodes with the lower frequency eigenmodes being filtered out. In all cases, the highest frequency eigenmode persists for all possible values of  $r$  on  $(0, 1]$ .

**2.2.1 A single defect** For the case of a single defect located at the origin,  $\mathcal{G}$  is a scalar:

$$\mathcal{G}(\omega) = \frac{1}{\alpha\pi} K\left(\frac{4}{\alpha^2}\right), \quad (32)$$

where  $K(x)$  is the complete elliptical integral of the first kind. The solveability condition may be written as

$$r = 1 + \pi \left( \frac{2}{\omega^2} - \frac{1}{2} \right) \left[ K\left(\frac{16}{(\omega^2 - 4)^2}\right) \right]^{-1}, \quad (33)$$

which has the leading order asymptotic representation

$$r \sim \frac{4}{\omega^2}, \quad \text{as } \omega \rightarrow \infty. \quad (34)$$

It is observed that (31) for the case of a single particle ( $N = 1$ ) agrees precisely with the leading order high frequency asymptotic expansion. Hence, the coalescence of the red and blue curves in figure 3a.

The localised defect mode is shown in figure 4a, together with field along the line  $n_2 = 0$  and the associated asymptotic field as  $n_1 \rightarrow \infty$  in figure 4b. Figures 4c and 4d show the field (solid blue line) and the band edge (in the vicinity of  $\alpha = 2$ ) asymptotics (dashed red) for a value of  $\alpha = 2.006$ . The asymptotic expansions show good agreement with the computed field, even for the far field asymptotics in the neighbourhood of the defect.



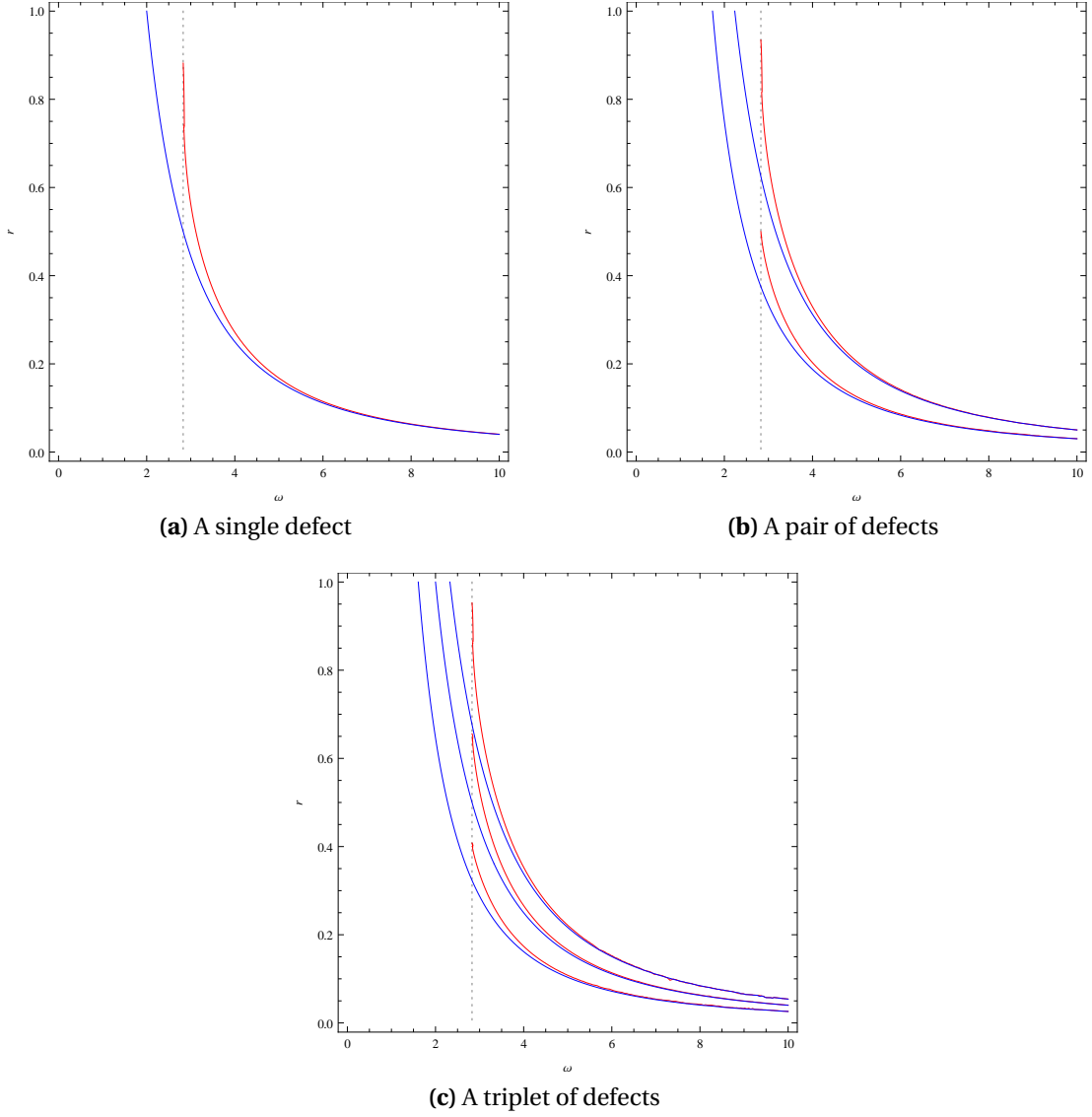


**Figure 3:** The red curves show the  $(\omega, r)$  values where the necessary and sufficient condition for a localised mode (cf. equation (11)) is satisfied. The blue curves show the corresponding values for a finite line of  $N$  masses.

**2.2.2 A pair of defects** In the case of a pair of defects,  $\mathcal{G}(\omega)$  is a  $2 \times 2$  matrix with the diagonal elements given by (32). The off-diagonal elements have the form

$$[\mathcal{G}(w)]_{12} = \frac{1}{4} - \frac{1}{2\pi} K \left( \frac{4}{\alpha^2} \right). \quad (35)$$

The solvability condition is

$$r_1 = 1 - \frac{4\pi(w^2 - 4)}{w^2\pi(w^2 - 4) - 2\omega^2(w^2 - 8)K \left[ \frac{16}{(-4 + w^2)^2} \right]}, \quad (36)$$

$$r_2 = 1 + \frac{4\pi(\omega^2 - 4)}{\pi\omega^2(\omega^2 - 4) - 2\omega^4 K \left( \frac{16}{(-4 + \omega^2)^2} \right)}, \quad (37)$$

whence the leading order high frequency asymptotic expansions are

$$r_1 \sim \frac{3}{\omega^2} \quad \text{and} \quad r_2 \sim \frac{5}{\omega^2} \quad \text{as} \quad \omega \rightarrow \infty, \quad (38)$$

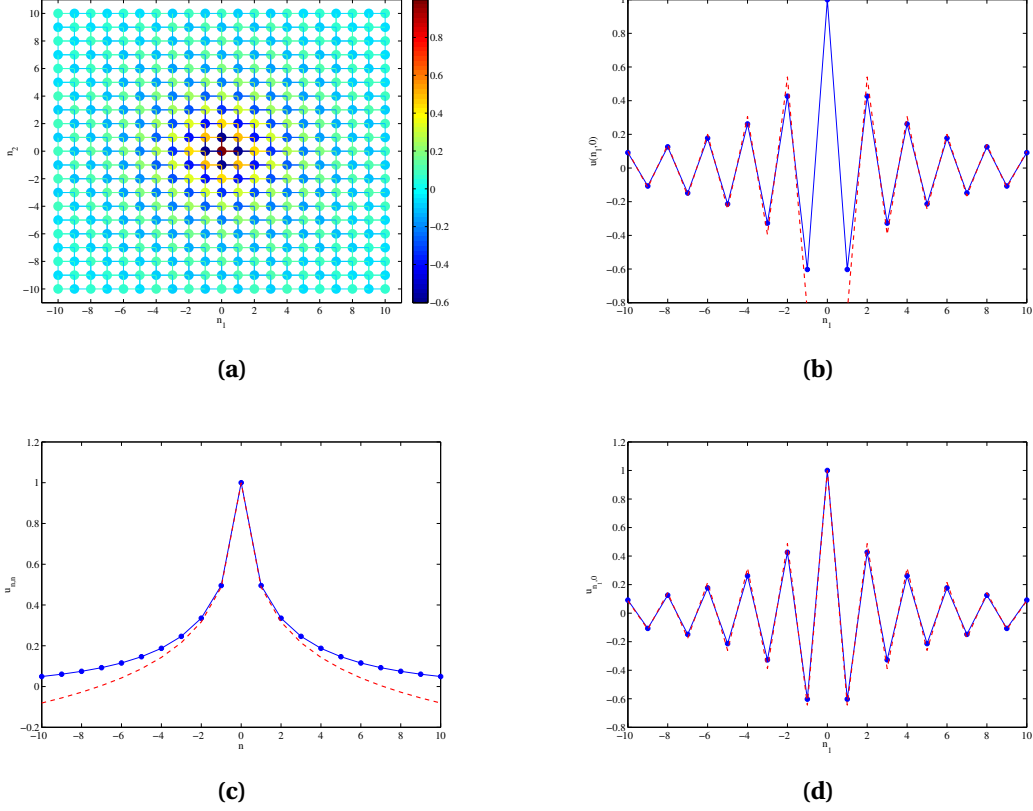


**Figure 4:** (a) The localised defect mode for a single defect with  $r = 0.8$  and  $\omega = 2.83$ . (b) The solid blue curve is the out of plane displacement along the line  $n_2 = 0$  and the red dashed curve is the asymptotic expansion for  $n_1 \rightarrow \infty$  (cf. (20)). (c) The out-of plane displacement along the line  $n_1 = n_2$  (solid blue curve) with the corresponding asymptotic expansion for the band edge (dashed red curve). (d) As for (b), but the dashed red curve represents the band edge expansion along  $n_2 = 0$ .

which again, agree precisely with the solvability condition of isolated system (31) for  $N = 2$ . Hence, the coalescence of the red and blue curves in figure 3.

Figure 5 shows the two defect modes together with field along the lines  $n_1 = 0$ , and  $n_2 = 0$  and the associated asymptotic field at infinity. In addition, the fuchsia dash-dot line in figure 5c shows the band edge expansion in the vicinity of  $\alpha = 2$ . In this case, figure 5c corresponds to value of  $\alpha \approx 2.025$ . Once again, the asymptotics are in good agreement with the computed field. Due to the symmetry, the field along the line  $n_1 = 1$  is identical to figure 5e for the symmetric case and identical up to a reflection in the line  $u_{0,n_2} = 0$  in figure 5f for the skew-symmetric case.

The lower red curve in figure 3b corresponds to  $r_1$  as defined in (36). The intersection of the lower red curve is given by

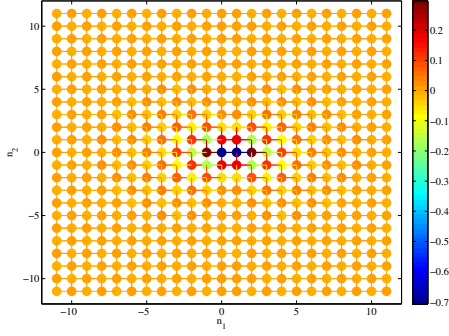
$$r_1^{(\max)} = \lim_{\omega \rightarrow \sqrt{8}} r_1 = \frac{1}{2}. \quad (39)$$

Hence for a pair of defects, a symmetric localised mode cannot be initiated for  $r \geq 1/2$ .

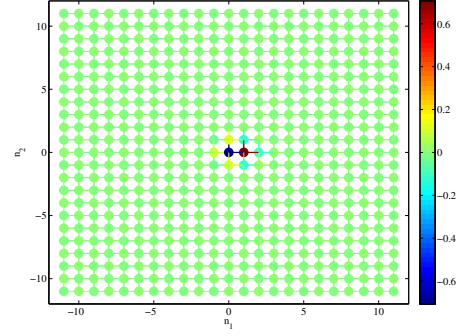
**2.2.3 A triplet of defects** For the case of three defects, the  $3 \times 3$   $\mathcal{G}$  matrix has the  $[\mathcal{G}]_{11}$  and  $[\mathcal{G}]_{12}$  elements as defined in equations (32) and (35). The remaining independent component is

$$[\mathcal{G}(w)]_{13} = [\mathcal{G}(\omega)]_{11} - \frac{\alpha}{2} + \frac{\alpha}{\pi} E\left(\frac{4}{\alpha^2}\right), \quad (40)$$

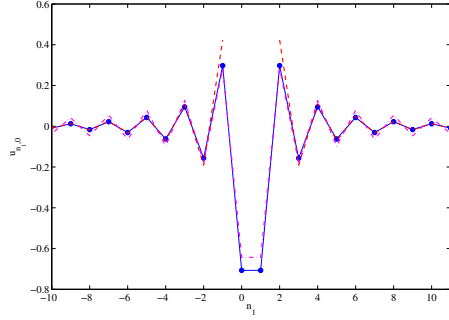
where  $E(x)$  is the complete Elliptic Integral of the second kind. The solvability condition is of similar form to the previous two cases, but cumbersome, and is therefore omitted for brevity. The



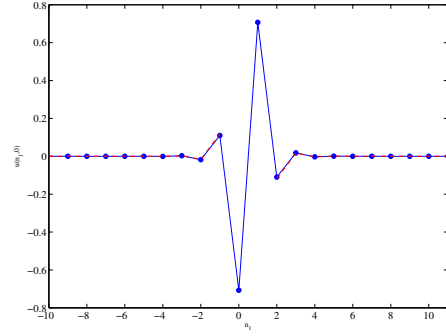
(a) Symmetric mode at  $\omega = 2.84$



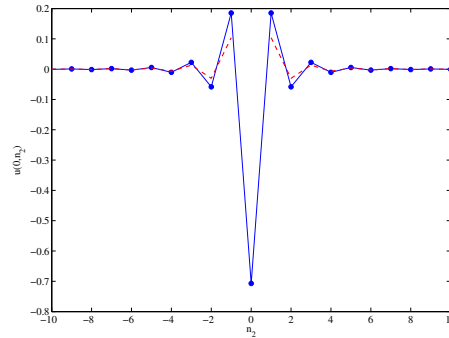
(b) Skew-symmetric mode at  $\omega = 3.35$



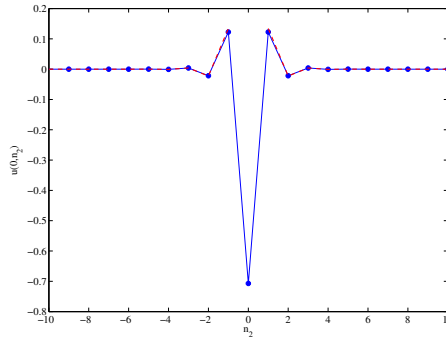
(c) The field along the line  $n_2 = 0$  for the symmetric mode



(d) The field along the line  $n_2 = 0$  for the skew-symmetric mode



(e) The field along the line  $n_1 = 0$  for the symmetric mode



(f) The field along the line  $n_1 = 0$  for the skew-symmetric mode

**Figure 5:** The localised defect mode for a pair of defects with  $r = 0.49$ . The blue curves are the out of plane displacement along the indicated line, and the red dashed curves are associated the asymptotic expansions in the far field. The dot-dash fuchsia curve in figure 5c shows the band edge expansion (cf. equation (28a)).

high frequency asymptotics for  $r(\omega)$  are

$$r_1 \sim \frac{4 - \sqrt{2}}{\omega^2}, \quad r_2 \sim \frac{4}{\omega^2}, \quad \text{and} \quad r_3 \sim \frac{4 + \sqrt{2}}{\omega^2} \quad \text{as} \quad \omega \rightarrow \infty, \quad (41)$$

which again coincide with (31) for the case of a particle triplet ( $N = 3$ ). The intersections of  $r_i(\omega)$  with the line  $\omega = \sqrt{8}$  are  $r_1^{(\max)} = 1 - 3\pi/16$ ,  $r_2^{(\max)} = 7/8 - (8 - 4\pi)^{-1}$ , and  $r_3^{(\max)} = 1$ .

The three localised eigenmodes, along with plots of the associated asymptotic expressions are shown in figure 6. Plots of the displacement field along the lines  $n_2 = 0$ ,  $n_1 = 1$  and  $n_1 = 0$  are shown. The fuchsia dash-dot line in figure 6c shows the band edge expansion in the vicinity of  $\alpha = 2$ . In this case, figure 5c corresponds to value of  $\alpha \approx 2.017$ . There are two symmetric modes (the lowest and highest frequency modes) and a single skew-symmetric mode, as expected from the properties of  $\mathcal{G}$  discuss in the previous subsection. However, for defects of mass  $r \geq r_1^{(\max)}$ , it is not possible to initiate the lower frequency symmetric eigenmode and only a further symmetric mode and a skew-symmetric mode persist. For values of  $r \geq r_2^{(\max)}$ , it is only possible to initiate the highest frequency symmetric mode.

### 3 A lattice containing an infinite chain of contrasting mass

Here, similar to [1], wave dispersion due to an infinite chain of particles embedded into a lattice, having a contrast in mass from the ambient lattice is considered.

A square lattice having particles of mass  $m$ , with positions  $k \in \mathbb{Z}, |n| \geq 1$ , is assumed to contain a chain of particles of mass  $M$  at  $n = 0$ . All bonds connecting the particles have stiffness  $\mu$  (see Figure 7). Both anti-symmetric and symmetric modes about the chain of masses at  $n = 0$ , are studied here. In other words, let  $u_{k,n}$  denote the displacement of the particle with position  $(k, n)$  in the lattice, then

$$u_{k,n} = -u_{k,-n} \quad \text{for } k, n \in \mathbb{Z} \quad (\text{anti-symmetric mode}) \quad (42)$$

$$u_{k,n} = u_{k,-n} \quad \text{for } k, n \in \mathbb{Z} \quad (\text{symmetric mode}). \quad (43)$$

Then by solving the problem in the upper half of the lattice ( $n \geq 0$ ), the solution can be extended to the lower half of the lattice.

#### 3.1 Equations of motion

The equation of motion for a particle with  $k \in \mathbb{Z}, n \geq 1$  is:

$$m \frac{d^2 u_{k,n}}{dt^2} = \mu(u_{k+1,n} + u_{k-1,n} + u_{k,n+1} + u_{k,n-1} - 4u_{k,n}) \quad (44)$$

and for  $k \in \mathbb{Z}, n = 0$ :

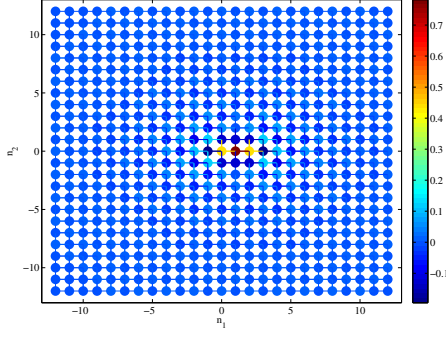
$$M \frac{d^2 u_{k,0}}{dt^2} = \mu(u_{k+1,0} + u_{k-1,0} + u_{k,1} + u_{k,-1} - 4u_{k,0}), \quad (45)$$

where the form of the last equation will vary depending on which of the conditions (42), (43) about  $n = 0$  is imposed.

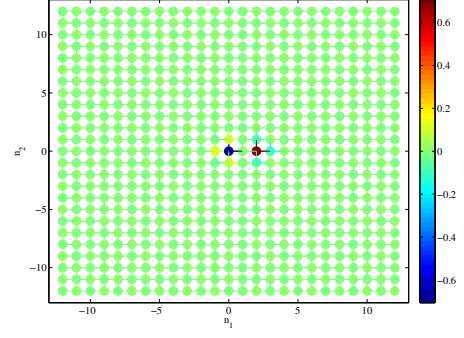
Since the geometry in Figure 7 is periodic in the horizontal direction, the solution  $u_{k,n}$  is sought in the form

$$u_{k,n} = U_n e^{i(kx - \omega t)}, \quad (46)$$

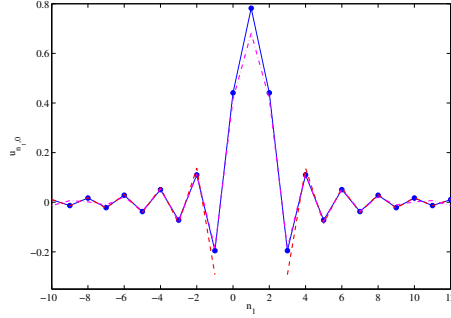
where  $\omega > 0$  is the angular frequency,  $x$  is the Bloch parameter in the horizontal direction which is considered here to be real and  $U_n$  is the amplitude. Insertion of this into (44) and (45), with



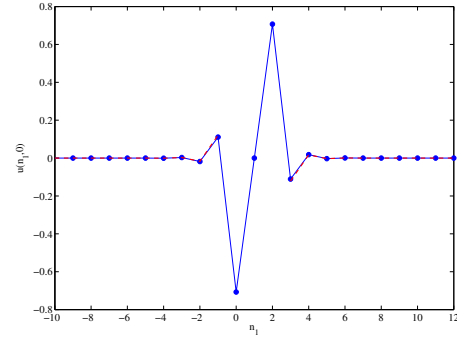
(a) Symmetric mode at  $\omega = 2.83$



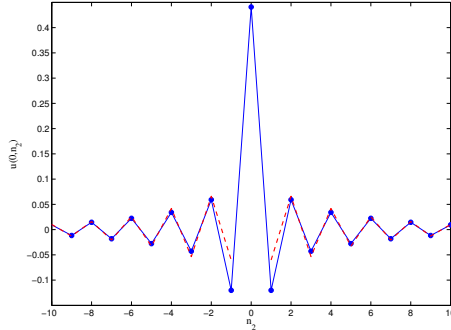
(b) Skew-symmetric mode at  $\omega = 3.33$



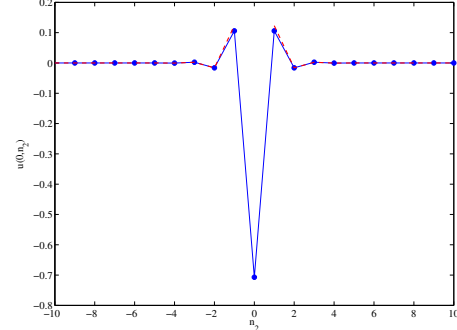
(c) The field along the line  $n_2 = 0$  for the symmetric mode



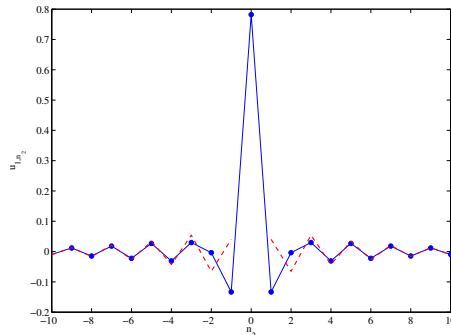
(d) The field along the line  $n_2 = 0$  for the skew-symmetric mode



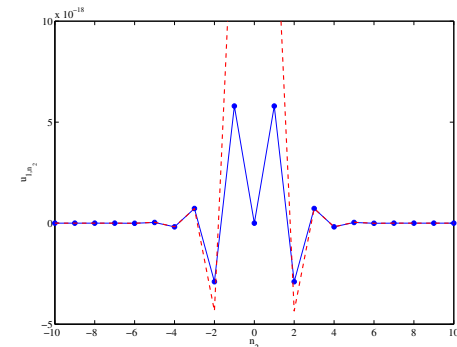
(e) The field along the line  $n_1 = 0$  for the symmetric mode



(f) The field along the line  $n_1 = 0$  for the skew-symmetric mode

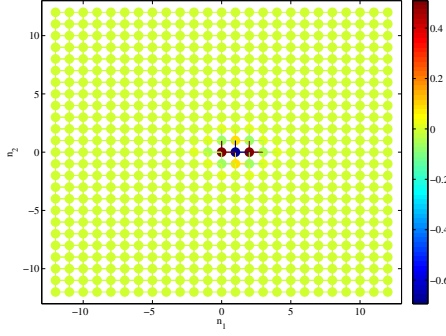


(g) The field along the line  $n_1 = 1$  for the symmetric mode

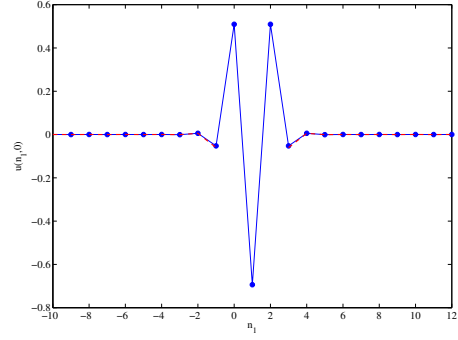


(h) The field along the line  $n_1 = 1$  for the skew-symmetric mode

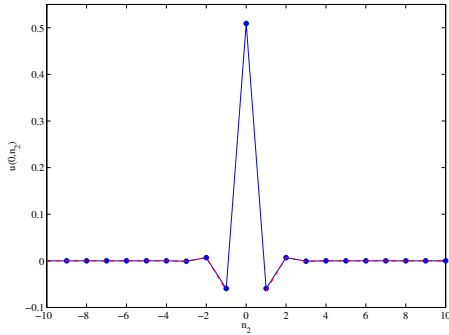
**Figure 6:** The localised defect mode for a pair of defects with  $r = 0.4$ . The blue curves are the out of plane displacement along the indicated line, and the red dashed curves are associated the asymptotic expansions in the far field. The fuchsia dash-dot line in figure 6a correspond to the band edge expansion (cf. equation (28a)).



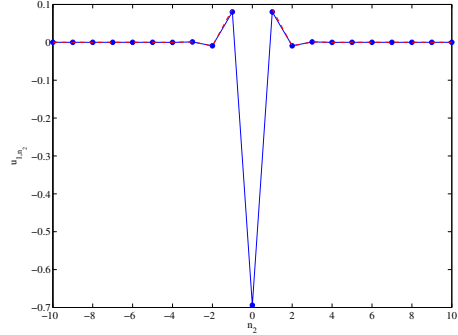
(i) The second symmetric mode at  $\omega = 3.77$



(j) The field along the line  $n_2 = 0$  for the second symmetric mode



(k) The field along the line  $n_1 = 0$  for the second symmetric mode



(l) The field along the line  $n_1 = 1$  for the second symmetric mode

**Figure 6:** The localised defect mode for a pair of defects with  $r = 0.4$ . The blue curves are the out of plane displacement along the indicated line, and the red dashed curves are associated the asymptotic expansions.

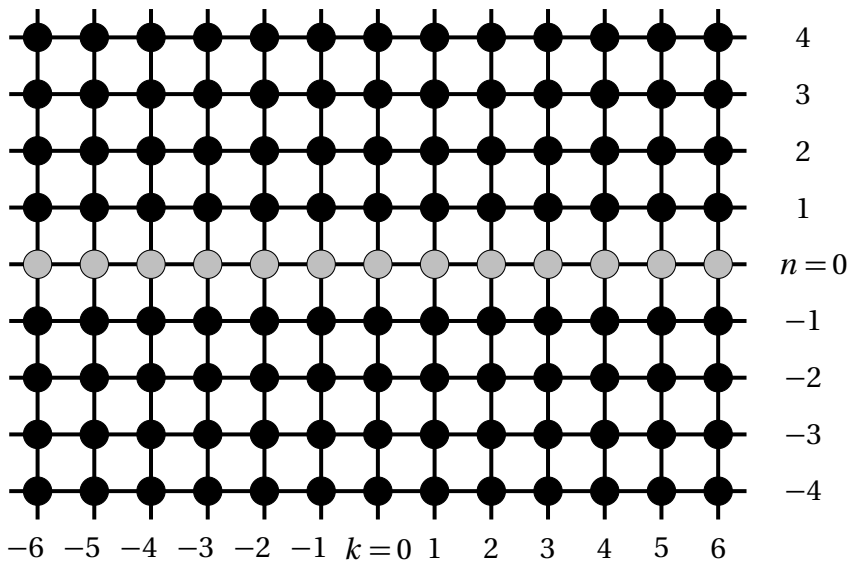


**Figure 7:** A square cell lattice containing a infinite chain of masses with mass  $M$  at  $n = 0$ , and the ambient lattice is composed of particles with mass  $m$ . All links are assumed to have stiffness  $\mu$ .

the introduction of the normalised frequency  $\omega = \sqrt{\mu/m} \omega_*$  and the mass contrast parameter  $r = M/m$ , gives

$$U_{n+1} + U_{n-1} - 2\Omega_1(\chi, i\omega_*)U_n = 0 \quad (n \geq 1), \quad (47)$$

$$U_1 + U_{-1} - 2\Omega_r(\chi, i\omega_*)U_0 = 0 \quad (n = 0), \quad (48)$$

where

$$\Omega_a(\chi, z) = 1 + 2 \sin^2(\chi/2) + \frac{az^2}{2}. \quad (49)$$

### 3.2 Anti-symmetric mode

The conditions (42) imply  $u_{k,0} = 0$  and consequently  $U_0 = 0$ . They also imply  $U_1 = -U_{-1}$ . Therefore in this case equation (48) is identically zero.

The solution for  $n \geq 2$  is then sought in the form

$$U_n = \lambda^n U_1, \quad |\lambda| \leq 1, \quad (50)$$

and for  $n \leq -2$ ,

$$U_n^{F*} = -\lambda^n U_1^{F*}. \quad (51)$$

Here the condition  $|\lambda| < 1$  gives the localised displacement field about the chain of masses at  $n = 0$ , and this field decays in the direction perpendicular to this line. The case  $|\lambda| = 1$  gives a field which propagates sinusoidally with constant amplitude away from  $n = 0$  in the transverse direction.

Combining (47) with (50) leads to

$$\lambda^2 - 2\Omega_1(\chi, i\omega_*)\lambda + 1 = 0. \quad (52)$$

The solution of (52) is

$$\lambda = \begin{cases} \Omega_1(\chi, i\omega_*) - \text{sign}(\Omega_1(\chi, i\omega_*))\sqrt{\Omega_1(\chi, i\omega_*)^2 - 1} & \text{for } |\Omega_1(\chi, i\omega_*)| > 1, \\ \pm 1 & \text{for } \Omega_1(\chi, i\omega_*) = \pm 1, \\ \Omega_1(\chi, i\omega_*) \pm i\sqrt{1 - \Omega_1(\chi, i\omega_*)^2} & \text{for } |\Omega_1(\chi, i\omega_*)| < 1. \end{cases} \quad (53)$$

It follows from (53) that for  $|\Omega_1(\chi, i\omega_*)| > 1$ ,  $|\lambda| < 1$ ; also if  $|\Omega_1(\chi, i\omega_*)| \leq 1$ , then note that  $|\lambda| = 1$ .

Recalling that the anti-symmetry condition (42) gives  $U_0 = 0$ , and substituting (50) in (47) for  $n = 1$ , leads to

$$(\lambda - 2\Omega_1(\chi, i\omega_*))U_1 = 0.$$

For a nontrivial solution for  $U_1$ , it follows from this equation that

$$\lambda - 2\Omega_1(\chi, i\omega_*) = 0. \quad (54)$$

Since it is required  $|\lambda| \leq 1$ , this equation implies that  $|\Omega_1(\chi, i\omega_*)| \leq 1/2$  in order for there to be a solution. According to (53), for  $|\lambda| < 1$ ,  $|\Omega_1(\chi, i\omega_*)| > 1$ , and so the only case to treat is  $|\lambda| = 1$ ,  $|\Omega_1(\chi, i\omega_*)| \leq 1/2$ , which again by (53) is only possible when  $\lambda$  is complex ( $|\Omega_1(\chi, i\omega_*)| < 1$ ). Then if  $\lambda$  is complex, for a solution of (54),  $\Omega_1(\chi, i\omega_*)$  must be complex with modulus less than or equal to  $1/2$ , which requires  $\omega_*$  to also be complex. Therefore there exist no real solutions of (54) for  $\omega_*$ .

### 3.3 Symmetric mode

As before, relations (50)–(53) hold for  $n \geq 2$ . The condition (43) now implies  $U_1 = U_{-1}$ . Then equation (47) for  $n = 1$  and (48) give the system

$$U_0 + (\lambda - 2\Omega_1(\chi, i\omega_*))U_1 = 0 \quad (n = 1), \quad (55)$$

$$U_1 - \Omega_r(\chi, i\omega_*)U_0 = 0 \quad (n = 0),$$

where (50) has already been used. Using matrix notations

$$\mathcal{S}_r(\chi, i\omega_*)\mathbf{u} = 0, \quad (56)$$

with

$$\mathcal{S}_r(\chi, i\omega_*) = \begin{pmatrix} \lambda - 2\Omega_1(\chi, i\omega_*) & 1 \\ 1 & -\Omega_r(\chi, i\omega_*) \end{pmatrix} \quad \text{and} \quad \mathbf{u} = (U_1, U_0)^T.$$

For non-trivial solutions  $U_j$ ,  $j = 0, 1$ , of (56), it is required

$$\det(\mathcal{S}_r(\chi, i\omega_*)) = 0,$$

which leads to

$$\Omega_r(\chi, i\omega_*)(\lambda - 2\Omega_1(\chi, i\omega_*)) + 1 = 0,$$

or

$$\frac{\Omega_r(\chi, i\omega_*)}{\lambda}(\lambda^2 - 2\Omega_1(\chi, i\omega_*)\lambda) + 1 = 0.$$

Then this with (52) yields the equation

$$\lambda - \Omega_r(\chi, i\omega_*) = 0. \quad (57)$$

### 3.4 Dispersion relations

For the solvability of (57), several scenarios are now discussed in detail:

**3.4.1 Solution with constant amplitude** a) *The case  $\lambda = \pm 1$ .* This corresponds to the case  $\Omega_1(\chi, i\omega_*) = \pm 1$ , and when solving this equation for  $\omega_*$ , this occurs when

$$\omega_*^{(1)}(\chi) = 2|\sin(\chi/2)|, \quad (\Omega_1(\chi, i\omega_*) = 1), \quad (58)$$

or

$$\omega_*^{(2)}(\chi) = 2\sqrt{1 + \sin^2(\chi/2)}, \quad (\Omega_1(\chi, i\omega_*) = -1). \quad (59)$$

Also, from (57), the equation

$$\Omega_r(\chi, i\omega_*) = \pm 1.$$

must be solved for  $\omega_*$ . This leads to the solutions  $\omega_*^{(3)}(\chi) = r^{-1/2}\omega_*^{(1)}(\chi)$ ,  $(\Omega_r(\chi, i\omega_*) = 1)$  and  $\omega_*^{(4)}(\chi) = r^{-1/2}\omega_*^{(2)}(\chi)$ ,  $(\Omega_r(\chi, i\omega_*) = -1)$ .

Returning to the original parameter  $\omega = \sqrt{\frac{\mu}{m}}\omega_*$ , there are four relations, they are

$$\omega_{1,m}(\chi) = \sqrt{\frac{\mu}{m}}\omega^{(1)}(\chi), \quad (\Omega_{m/\mu}(\chi, i\omega) = 1), \quad (60)$$

$$\omega_{2,m}(\chi) = \sqrt{\frac{\mu}{m}}\omega^{(2)}(\chi), \quad (\Omega_{m/\mu}(\chi, i\omega) = -1), \quad (61)$$



$$\omega_{1,M}(\chi) \quad (\Omega_{M/\mu}(\chi, i\omega) = 1), \quad \text{and} \quad \omega_{2,M}(\chi) \quad (\Omega_{M/\mu}(\chi, i\omega) = -1). \quad (62)$$

It follows that  $\Omega_1(\chi, i\omega) = \Omega_r(\chi, i\omega) = \pm 1$  if and only if  $r = 1$ . Then for  $0 < r < 1$ , this means (57) will have no real solutions for  $\omega$ . Therefore there are no solutions with constant amplitude for the case  $\lambda = \pm 1$  and  $r < 1$ .

b) *The case when  $\lambda$  is complex.* For  $\lambda$  to be complex, the condition  $|\Omega_1(\chi, i\omega_*)| < 1$  has to be satisfied, and then  $|\lambda| = 1$ . Since  $r \neq 1$  ( $m \neq M$ ), and  $\Omega_r(\chi, i\omega_*)$  is real for  $\omega_* > 0$  and  $\chi \in \mathbb{R}$ , then (57) has no real solutions for  $\omega_*$ . Note that  $|\Omega_1(\chi, i\omega_*)| < 1$  is satisfied for

$$\omega_*^{(1)}(\chi) < \omega_* < \omega_*^{(2)}(\chi).$$

**3.4.2 Localised defect modes** c) *The case  $|\lambda| < 1$ .* According to (53), this happens when  $|\Omega_1(\chi, i\omega_*)| > 1$ . For solutions to (57), it must also hold that  $|\Omega_r(\chi, i\omega_*)| < 1$ . Then (52) and (57) give the equation

$$\Omega_r(\chi, i\omega_*)^2 - 2\Omega_r(\chi, i\omega_*)\Omega_1(\chi, i\omega_*) + 1 = 0,$$

which by (49), is equivalent to

$$\frac{1}{4}r(r-2)\omega_*^4 + (1 + 2\sin^2(\chi/2))\omega_*^2 - 4\sin^2(\chi/2)(1 + \sin^2(\chi/2)) = 0. \quad (63)$$

This is a biquadratic equation in terms of  $\omega_*$ . The inequalities  $|\Omega_r(\chi, i\omega_*)| < 1$  and  $|\Omega_1(\chi, i\omega_*)| > 1$ , lead to

$$r^{-1/2}\omega_*^{(1)}(\chi) < \omega_* < r^{-1/2}\omega_*^{(2)}(\chi) \quad (64)$$

together with

$$\omega_*^{(1)}(\chi) > \omega_* \quad \text{or} \quad \omega_* > \omega_*^{(2)}(\chi). \quad (65)$$

Either of the last two inequalities gives  $|\lambda| < 1$ , and when one of these inequalities is taken with (64), the solutions of (57) for  $\omega$  should satisfy these conditions. In obtaining a solution to (63), conditions (64) and (65) should be verified to determine the dispersion relations, that are solutions of the original equation (57).

First note that for localised modes (64) and (65) yield either

$$\omega_*^{(2)}(\chi) < r^{-1/2}\omega_*^{(2)}(\chi), \quad \text{for all } \chi \in \mathbb{R},$$

which leads to  $r < 1$  ( $M < m$ ), or

$$r^{-1/2}\omega_*^{(2)}(\chi) < \omega_*^{(1)}(\chi), \quad \text{for all } \chi \in \mathbb{R},$$

which is never satisfied for any  $r$ .

**3.4.3 Roots of the extended equation (63) and asymptotics** The solutions of (63) are:

$$\omega_*^{(\pm)}(\chi) = \left\{ \frac{2}{r(2-r)} \left[ 1 + 2\sin^2(\chi/2) \pm \sqrt{1 + 4(r-1)^2 \sin^2(\chi/2)(1 + \sin^2(\chi/2))} \right] \right\}^{1/2}, \quad \text{for } 0 < r < 1, \quad (66)$$

$$\omega_*^{(+)}(\chi) = 2|\sin(\chi/2)| \sqrt{\frac{1 + \sin^2(\chi/2)}{1 + 2\sin^2(\chi/2)}}, \quad \text{for } r = 0. \quad (67)$$

Using (66), for  $r \rightarrow 0$  ( $M \rightarrow 0$ ):

$$(\omega_*^{(+)}(\chi))^2 = \frac{4 \sin^2(\chi/2)(1 + \sin^2(\chi/2))}{1 + 2 \sin^2(\chi/2)} + O(r).$$

Here the leading order term is equivalent to (67). Also

$$(\omega_*^{(-)}(\chi))^2 = \frac{2}{r}(1 + 2 \sin^2(\chi/2)) - \frac{1 + 8 \sin^2(\chi/2) + 8 \sin^4(\chi/2)}{1 + 2 \sin^2(\chi/2)} + O(r),$$

where, the second term is bounded and negative, whereas the first term dominates for  $r \rightarrow 0$  ( $M \rightarrow 0$ ) and so in this limit  $\max_{\chi \in \mathbb{R}} \{\omega_*^{(-)}(\chi)\} \rightarrow \infty$ .

**3.4.4 Roots of the (57)** Now it will be verified if the solutions (66) of the extended equation (63), satisfy (64) and (65) and are consequently roots of (57).

*The function  $\omega_*^{(-)}$ .* Owing to the inequality  $ab \leq 2^{-1}(a^2 + b^2)$ ,

$$\sqrt{1 + 4(r-1)^2 \sin^2(\chi/2)(1 + \sin^2(\chi/2))} \leq 1 + 2(r-1)^2 \sin^2(\chi/2)(1 + \sin^2(\chi/2)),$$

and so from (66)

$$\begin{aligned} (\omega_*^{(-)}(\chi))^2 &\leq \frac{4}{r(2-r)}(1 + \sin^2(\chi/2))(1 + (r-1)^2 \sin^2(\chi/2)) \\ &\leq \frac{4}{r(2-r)}(1 + \sin^2(\chi/2))(1 + (r-1)^2), \end{aligned}$$

for any  $\chi \in \mathbb{R}$ . The last factor on the right is positive and convex, and for  $0 < r < 1$  is less than  $2 - r$ . Therefore

$$\omega_*^{(-)}(\chi) < r^{-1/2} \omega_*^{(2)}(\chi), \quad \text{for all } \chi \in \mathbb{R}. \quad (68)$$

Now, the function inside the radical of  $(\omega_*^{(-)})^2$  (see (66)), can be written as

$$(r-1)^2(2 \sin^2(\chi/2) + 1)^2 + 1 - (r-1)^2,$$

and this implies for  $0 < r < 1$  and  $\chi \in \mathbb{R}$ ,

$$(\omega_*^{(-)}(\chi))^2 > \frac{2}{r}(1 + 2 \sin^2(\chi/2)).$$

This then leads to

$$\omega_*^{(-)}(\chi) > r^{-1/2} \omega_*^{(1)}(\chi), \quad \chi \in \mathbb{R}. \quad (69)$$

Also note that due to the equality  $1 - (r-1)^2 = r(2-r)$ , it can be seen this function is concave and less than 1 for  $r < 1$ . Then using this fact,  $\omega_*^{(-)}$  can also be estimated from below:

$$\omega_*^{(-)}(\chi) > \omega_*^{(2)}(\chi), \quad \text{for all } \chi \in \mathbb{R}. \quad (70)$$

Then (68), (69) and (70) show that  $\omega_*^{(-)}$  satisfies inequalities (64) and (65)<sub>2</sub> and is therefore a solution of (57).

*The function  $\omega_*^{(+)}$ .* Next, it will be shown that  $\omega_*^{(+)}$  is not a solution the original equation (57), since  $|\Omega_r(\chi, i\omega_*^{(+)})| > 1$ . Indeed, since the function in the radical of  $(\omega_*^{(+)})^2$  is always positive

$$(\omega_*^{(+)}(\chi))^2 < \frac{4}{r(2-r)} \sin^2(\chi/2).$$

for  $\chi \in \mathbb{R}$ . Then, since  $r < 1$ , it can be asserted

$$\omega_*^{(+)}(\chi) < r^{-1/2} \omega_*^{(1)}(\chi), \quad \text{for } \chi \in \mathbb{R}.$$

Therefore,  $\omega_*^{(+)}$  does not satisfy (64) and is not a solution of (57).

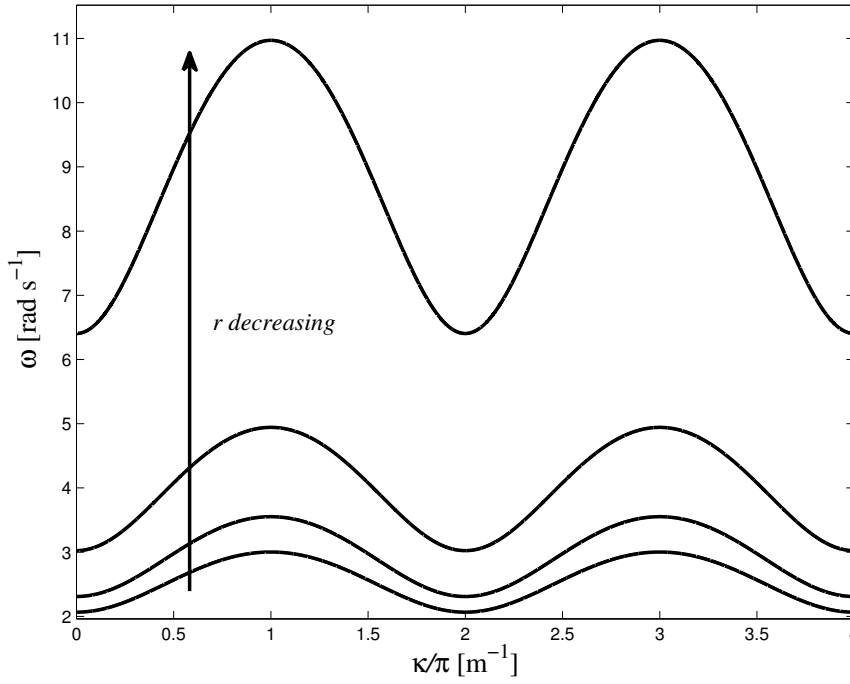


**Figure 8:** The dispersion relation  $\omega_-$ , given in (71) when  $m = \mu = 1$ , plotted as a function of the normalised Bloch parameter  $\kappa/\pi$  for  $r = 0.05, 0.25, 0.5$  and  $0.75$ .

**3.4.5 Dispersion relation when  $|\lambda| < 1$**  In terms of the original parameters  $\omega$ ,  $M$ ,  $m$ , the dispersion relation that satisfies  $|\Omega_1(\kappa, i\omega_*)| > 1$ ,  $|\Omega_r(\kappa, i\omega_*)| < 1$  for all  $\kappa \in \mathbb{R}$  and is a solution of (57) for  $0 < M < m$  is

$$\omega_-(\kappa) = \left\{ \frac{2\mu}{M(2m-M)} \left[ m(1 + 2\sin^2(\kappa/2)) + \sqrt{m^2 + 4(M-m)^2 \sin^2(\kappa/2)(1 + \sin^2(\kappa/2))} \right] \right\}^{1/2}, \quad (M < m). \quad (71)$$

In Figure 8, this expression is plotted for  $m = \mu = 1$  and several values of  $M$  (or contrast parameter  $r$ ). The in-phase standing wave solution, of the form (46), is always given when  $\kappa = 0$  and

$$\omega = \sqrt{\frac{4m\mu}{M(2m-M)}}, \quad (72)$$

whereas for the out-of-phase solution,  $\kappa = \pi$  and

$$\omega = \sqrt{\frac{2\mu}{M(2m-M)} [3m + \sqrt{m^2 + 8(M-m)^2}]}. \quad (73)$$

## 4 Numerical simulation for a long defect: the case of large $N$

In this section, the objective is to show that the range of eigenfrequencies for which localised eigenmodes exist for the model described in section 2, can be predicted using the model of an infinite chain of defects considered in section 3.

A defect composed of  $N = 20$  particles of mass  $r = M = 0.25$  is embedded within an infinite square lattice. The particles in the ambient lattice have mass  $m = 1$  and the bonds linking the particles have unit stiffness.

The eigenfrequencies of the finite defect were computed using the method described in section 2 and are shown in table 1.

In this table, the eigenfrequency  $\omega_{\max} = 3.0374$  corresponds to an in-phase standing wave solution, whereas the frequency  $\omega_{\min} = 4.9344$  represents the out-of-phase solution.

Eigenfrequencies				
3.0374	4.1558	3.0778	4.2906	3.1430
4.4171	3.2303	4.5335	3.3364	4.6378
3.4574	4.7286	3.5896	4.8045	3.7291
4.8646	3.8722	4.9081	4.0155	4.9344

**Table 1:** The eigenfrequencies of a line of 20 defects, with mass  $r = 0.25$ .

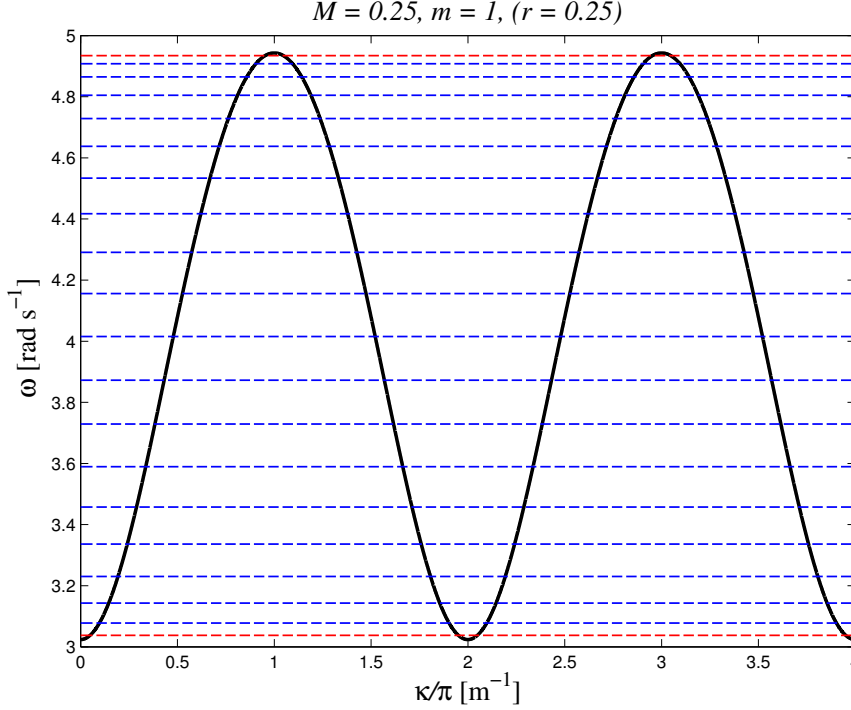


**Figure 9:** The dispersion relation (71), for the infinite chain, plotted as a function of the normalised Bloch parameter, for  $M = 0.25$ ,  $m = \mu = 1$ , represented by the solid curve. Also shown are straight-dashed lines corresponding to the the eigenfrequencies computed for a finite defect containing  $N = 20$  masses, found in table 1

Since  $N$  is large, it is useful to consider the model of an infinite chain embedded in a square lattice. Expressions (72) and (73) predict the values of the frequency  $\omega$  for which there exist such solutions, for the numerical values above. The in-phase solution occurs when  $\kappa = 0$  and  $\omega = 3.0237$ . The out-of-phase solution occurs when  $\kappa = \pi$  and  $\omega = 4.9432$ . These values of the frequency are close to those encountered in the problem of the finite defect for  $N = 20$ . Moreover, all the eigenfrequencies computed for the finite defect in table 1, lie within the passband for the infinite defect, as shown in Figure 9.

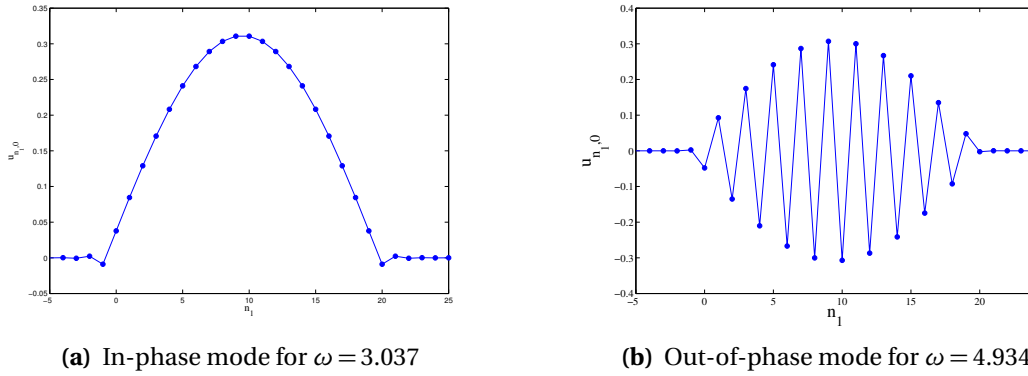


**Figure 10:** Eigenmodes for the maximum and minimum eigenfrequencies for a finite line containing 20 defects.

Figure 10 shows the plot of the eigenmodes for the maximum and minimum eigenfrequencies computed for the line defect containing 20 masses. The maximum eigenfrequency  $\omega_{\max}$  corresponds to the out-of-phase mode, whereas the minimum eigenfrequency  $\omega_{\min}$  gives the in-phase

mode.

## 5 Concluding remarks

A comparative analysis of two classes of problems has been presented: localised vibrations around a finite size defect created by a line of masses in a square lattice and an infinite waveguide represented by a chain of masses embedded into an ambient lattice.

Although the physical configurations and the methods of analysis of these problems are different, one may observe remarkable properties of solutions, which can be used to make a strong connection. As illustrated in figure 9, the pass band for frequencies of waveguide modes, localised around an infinite chain of masses in a square lattice, contains all eigenmodes describing vibrations localised around a rectilinear defect built of a finite number of masses embedded into the lattice.

Special attention is given to the band edges: figure 9 shows that the frequencies of the eigenmodes for a finite rectilinear defect are distributed non-uniformly and they cluster around the edges of the pass band identified for the infinite waveguide problem. Furthermore, the limit, as one approaches the band edge frequency, corresponds to a homogenisation approximation of the rectilinear defect as an inclusion embedded into a homogenised ambient system. The illustrative numerical simulation is produced for an array of 20 masses. However, the effect shown is generic, and with the increase of number of masses, the density of frequencies of localised modes near the band edges, identified for an infinite waveguide, increases.

Symmetric and skew-symmetric modes have been constructed and analysed for a rectilinear “inclusion” built of a finite number of masses embedded into the lattice. It has also been shown that the total force produced by the vibrating discrete inclusion on the ambient lattice equals zero for all skew-symmetric modes. Consequently, the displacement fields associated with skew-symmetric modes decay at infinity like dipoles, vanishing faster than the displacements corresponding to symmetric modes. This follows from the analytical representations for the solutions and illustrated in figure 5 and 6 where the skew-symmetric modes appear to be localised to a much higher degree than symmetric modes. In the aforementioned numerical simulations, skew-symmetric and symmetric modes appear in pairs, and the frequency of the skew-symmetric mode is higher than the frequency of the corresponding symmetric mode.

Finally, we would like to comment on the symmetric and skew-symmetric eigenmodes for a chain of 20 masses shown in figure 10. The corresponding frequencies are the maximum and minimum values among the array of frequencies associated with horizontal lines in figure 9. The envelope curves for both diagrams in figure 10 represent the first eigenmode of a homogenised rectilinear inclusion. As expected, the skew-symmetric mode of figure 10b has the higher frequency than the symmetric mode of figure 10a.

## Acknowledgements

The authors wish to thank Professor R.C. McPhedran for his invaluable discussions and electronic correspondence. D.J.C., A.B.M. & N.V.M. acknowledge the financial support of EPSRC grant number EP/H018514/1. M.J.N. & I.S.J. acknowledge the financial support of EPSRC grant number EP/H018239/1.

## References

- [1] G.G. Osharovich and M.V. Ayzenberg-Stepanenko. Wave localization in stratified square-cell lattices: The antiplane problem. *Journal of Sound and Vibration*, 331:1378–1397, 2012.
- [2] L.I. Slepyan. *Models and Phenomena in Fracture Mechanics*. Springer-Verlag Berlin Heidelberg New York, 2002.

- [3] G.S. Mishuris, A.B. Movchan, and L.S. Slepyan. Localised knife waves in a structured interface. *Journal of the Mechanics and Physics of Solids*, 57:1958–1979, 2009.
- [4] R. V. Craster, J. Kaplunov, and J. Postnova. High-Frequency Asymptotics, Homogenisation and Localisation for Lattices. *The Quarterly Journal of Mechanics and Applied Mathematics*, 63(4):497–519, 2010.
- [5] M. Ayzenberg-Stepanenkov and L. Slepyan. Resonant-frequency primitive waveforms and star waves in lattices. *Journal of Sound and Vibration*, 313(3-5):812–821, June 2008.
- [6] DJ Colquitt, I. S. Jones, N. V. Movchan, and A.B. Movchan. Dynamic anisotropy and localization in elastic lattice systems. *Waves in Random and Complex Media*, 22(2):143–159, 2012.
- [7] P. Martin. Discrete scattering theory: Green's function for a square lattice. *Wave Motion*, 43(7):619–629, 2006.
- [8] A.B. Movchan and L. Slepyan. Band gap Green's functions and localized oscillations. *Proceedings of the Royal Society A: Mathematical, Physical and Engineering Sciences*, 463(2086):2709–2727, 2007.
- [9] A.A. Maradudin. Some effects of point defects on the vibrations of crystal lattices. *Reports on Progress in Physics*, 28:331–380, 1965.
- [10] S. Mahmoodian, R. C. McPhedran, C. de Sterke, K. Dossou, C. Poulton, and L. Botten. Single and coupled degenerate defect modes in two-dimensional photonic crystal band gaps. *Physical Review A*, 79(1):1–12, 2009.
- [11] KB Dossou, LC Botten, R. C. McPhedran, and CG Poulton. Shallow defect states in two-dimensional photonic crystals. *Physical Review A*, 77:1–18, 2008.
- [12] B. van der Pol and H. Bremmer. *Operational Calculus based on the two-sided Laplace Transform*. Cambridge University Press, London, 1950.
- [13] A.P. Prudnikov, Yu. A. Brychkov, and O.I. Marichev. *Integrals and Series*, volume 4. Gordon and Breach Science Publishers, Amsterdam, 1992.
- [14] A. Cantoni and P. Butler. Eigenvalues and Eigenvectors of Symmetric Centrosymmetric Matrices. *Linear Algebra and its applications*, 13:275–288, 1976.
- [15] W. Bühring. Generalized hypergeometric functions at unit argument. *Proceedings of the American Mathematical Society*, 114(1):pp. 145–153, 1992.
- [16] M. Saigo and H. M. Srivastava. The behavior of the zero-balanced hypergeometric series  ${}_pF_{p-1}$  near the boundary of its convergence region. *Proceedings of the American Mathematical Society*, 110(1):pp. 71–76, 1990.